Investigation of Optimal Gating Envelope Size for Automatic Gating in MR-Guided Radiotherapy

Jeon, Mijin

Department of Integrative Medicine
Graduate School
Yonsei University

Investigation of Optimal Gating Envelope Size for Automatic Gating in MR-Guided Radiotherapy

Advisor Kim, Jihun

A Master's Thesis Submitted
to the Department of Integrative Medicine
and the Committee on Graduate School
of Yonsei University in Partial Fulfillment of the
Requirements for the Degree of
Master of Digital Healthcare

Jeon, Mijin

June 2025

Investigation of Optimal Gating Envelope Size for Automatic Gating in MR-Guided Radiotherapy

This Certifies that the Master's Thesis of Jeon, Mijin is Approved

Committee Chair	**Kim, Jihun**
Committee Member	**Kim, Jun Won**
Committee Member	**Hong, Chae-Seon**

Department of Integrative Medicine
Graduate School
Yonsei University
June 2025

TABLE OF CONTENTS

LIST OF FIGURES ····· iii

LIST OF TABLES ····· iv

ABSTRACT ····· v

1. INTRODUCTION ····· 1

2. MATERIAL AND METHODS ····· 3

2.1. Patient Selection and Imaging Acquisition ····· 3

2.2. Definition of Gating Envelopes ····· 6

2.3. Dosimetric Analysis ····· 8

2.4. Simulation of Automatic Gating Treatment ····· 11

2.5. Case-Specific Analysis ····· 13

3. RESULTS ····· 14

3.1. Dosimetric Impact of Gating Envelope Size ····· 14

3.2. Impact on Beam-on-Time Efficiency ····· 19

3.3. Case-Specific Analysis ····· 22

3.3.1. Case I: Tumor adjacent to the liver dome ····· 22

3.3.1. Case II: Extensive tumor motion ····· 23

3.3.1. Case III: Tumor in close proximity to organs-at-risk ····· 24

4. DISCUSSION ····· 26

5. CONCLUSIONS ····· 29

REFERENCES ····· 30

국문요약 ····· 33

LIST OF FIGURES

<Fig 1> Axial 3D planning CT images showing the GTV (red contour) for each of the 10 patients. 5

<Fig 2> (a) Coronal, (b) sagittal, and (c) axial CT images illustrating the GTV (red) and ITVs generated to cover different ranges of respiratory phases: ITV (0-90%, yellow), ITV 7-phase (20-80%, cyan), ITV 5-phase (30-70%, green), and ITV 3-phase (40-60%, pink). 7

<Fig 3> Schematic illustration of the GTV-to-OAR distance. The dashed line represents a uniformly expanded contour from the GTV, where the expansion continues until the expanded contour becomes tangent to the OAR contour. In this illustrative case, where the OAR overlapps with the PTV, a negative value is assigned to the GTV-to-OAR distance. 10

<Fig 4> Operational view of a vendor-provided motion tracking software package, Motion Monitoring Research Package (MMRP), where the upper panel displays axial, sagittal, and coronal cine MR images with the GTV (red) and the GE (yellow) overlaid, and the lower panel shows (a) motion tracking results (translations) in three directions and (b) calculation results of beam-on-time efficiency (represented as beam on (%) in MMRP), total treatment time, and beam-on-time. 12

<Fig 5> Comparison of the liver mean dose normalized to that of the ITV-based treatment plan between three GE conditions—7-phase GE (blue), 5-phase GE (orange), and 3-phase GE (gray). 15

<Fig 6> Liver mean dose as a function of GTV volume under different motion management strategies: ITV approach (orange), 7-phase GE (cyan), 5-phase GE (green), and 3-phase GE (pink). Horizontal dashed lines indicate QUANTEC liver dose limits: 28 Gy (gray), 18 Gy (black), and 15 Gy (blue), respectively. 16

<Fig 7> Normalized OAR doses (% of the prescription dose) plotted against the GTV-to-OAR distance (cm) for the stomach, duodenum, and bowel. Each data point represents one of four motion management techniques: ITV approach, gating treatment techniques with 7-phase, 5-phase, and 3-phase GEs. 18

<Fig 8> Box plot of comparing beam-on-time efficiency values calculated for all patients between three GE groups. 19

<Fig 9> Representation of a patient case with a tumor adjacent to the liver dome (Patient 1), whose GTV contours are overlaid on (a) coronal, (b) sagittal, and (c) axial slices of the CT scan. 22

<Fig 10> Representation of two representative cases (Patients 3 and 6) with relatively large tumor motions: coronal views of the 4D CT images at end-inhalation and end-exhalation respiratory phases (top panel), where two yellow lines represent the levels of the liver dome, and tumor motion traces in the superior-inferior direction (bottom). 23

<Fig 11> Representation of a patient case with a tumor in close proximity to gastrointestinal OARs (stomach, duodenum, and bowel); contours of the GTV and the OARs are overlaid on the axial (left), coronal (right-top), and sagittal (right-bottom) slices of the CT image. 25

LIST OF TABLES

<Table 1> Summary of patient characteristics. 4

<Table 2> Dose constraints for the liver and gastrointestinal OARs for various dose fractionation schemes based on the QUANTEC guidelines. 8

<Table 3> Comparison of target dose parameters across different motion management techniques: ITV approach and respiratory gating with various GE configurations. Values are presented as mean ± standard deviation. 14

<Table 4> Minimum distances between the GTV and adjacent OARs (stomach, duodenum, and bowel). Negative values indicate volumetric overlap between the radiation target (.e., PTV for ITV approach or GE for gating treatment) and the OAR. 17

<Table 5> Statistics of beam-on-time efficiency values calculated across all patients for each of the GE configurations. 20

<Table 6> Summary of the correlation analysis between various factors (GE sizes, GTV volume, and tumor motion magnitude in the SI direction (SI motion magnitude)): Spearman's rank correlation coefficients and the corresponding p-values. 20

ABSTRACT

Investigation of Optimal Gating Envelope Size for Automatic Gating in MRI-Guided Radiotherapy

This study aims to investigate the optimal gating envelope (GE) size for automatic gating in magnetic resonance imaging-guided radiotherapy (MRIgRT) for liver cancer. The effects of gating envelope size on distribution and treatment time efficiency were analyzed using real-time motion data calculated from cine MRI acquired during MRIgRT.

Imaging and radiation treatment data from ten liver cancer patients who underwent MRIgRT were retrospectively analyzed. For this patient cohort, in addition to the internal target volume-based treatment approach, a gating treatment approach was evaluated using three different GE sizes covering 7, 5, and 3 out of 10 respiratory phases (referred to as 7-phase, 5-phase, and 3-phase GEs, respectively). MRIgRT treatment plans were created for each of the motion management techniques and the resulting dosimetric quality was compared between the plans. Liver doses were analyzed in relation to the gross tumor volume (GTV) size. Doses to organs-at-risk (OARs), such the stomach, duodenum, and bowel, were evaluated by accounting for a distance between the radiation target and each of the OARs. Tumor motion trajectories were calculated using a rigid registration algorithm implemented in a vendor-provided motion analysis tool for automatic gating.

The results revealed a clear trade-off between treatment efficiency and normal tissue sparing depending on GE size. In patients with a GTV of 50-100 cc and a minimal GTV-to-OAR distance (< 1 cm), small GE significantly reduced mean liver dose and OAR exposure. Conversely, in patients with a smaller GTV and a greater anatomical separation, broader GE settings enabled higher beam-on ratios with acceptable dose constraints. A

significant correlation between GTV-to-OAR distance and normalized OAR dose was observed, underscoring the importance of patient-specific anatomical assessment in GE size determination.

This study highlights the clinical potential of individualized gating strategies informed by real-time motion analysis. Personalized GE optimization may enhance precision, improve organ sparing, and reduce treatment time in MR-guided radiotherapy for liver cancer.

Keywords: Magnetic resonance imaging-guided radiotherapy (MRIgRT), cine MRI, liver cancer, gating envelope, automatic gating, treatment efficiency, normal tissue sparing

1. Introduction

Radiation therapy is a cornerstone in the treatment of cancer, aiming to deliver high-dose radiation to malignant tissues while minimizing damage to surrounding healthy organs. Over the past few decades, technological advances such as three-dimensional conformal radiotherapy, intensity-modulated radiotherapy (IMRT), image-guided radiotherapy (IGRT), and particle therapy have significantly improved treatment precision (Bucknell, Belderbos et al., 2022). These modalities have demonstrated clinical benefit across a wide range of malignancies—including brain tumors, lung cancer, and prostate cancer—resulting in improved tumor control, symptom relief, and quality of life (Kong & Hong, 2016).

However, for tumors located in the thoracic and abdominal regions such as hepatocellular carcinoma (HCC) and lung cancer, respiratory-induced organ motion remains a major obstacle. To manage this challenge, several motion mitigation techniques have been developed: the use of internal target volume (ITV) to cover motion extent, abdominal compression device to restrict breathing, and gating technique using internal or external markers. Despite their clinical utility, these strategies present inherent drawbacks. ITV-based approaches may lead to over-irradiation of healthy tissue; abdominal compression may not be tolerable for all patients; internal markers require invasive procedures; and prolonged IGRT increases radiation exposure (Shirato, Shimizu et al., 2000).

In response to these limitations, magnetic resonance imaging-guided radiotherapy (MRIgRT) systems have been introduced, offering real-time, high-resolution imaging without additional radiation exposure. The integration of MRI with linear accelerators such as the ViewRay MRIdian (ViewRay, Inc., Cleveland, OH, USA) and Elekta Unity (Elekta AB, Stockholm, Sweden) enables continuous soft-tissue visualization and precise beam control. Real-time cine MRI facilitates direct tumor tracking during treatment, while

automated beam gating ensures that radiation is delivered only when the tumor is within a defined gating envelope (Kishan, Ma et al., 2023; Rogowski, von Bestenbostel et al., 2021). This capability enhances treatment accuracy and safety, particularly for mobile abdominal targets.

Despite these advantages, current clinical implementation of MRIgRT often relies on fixed margin settings that may not fully reflect individual respiratory variability. Specifically, previous studies utilized uniform margins for breath-hold gating (Rogowski, von Bestenbostel et al., 2021; Ehrbar, Käser et al., 2022). Other studies on MRIgRT under free-breathing conditions proposed population-based approaches to determine planning target volume (PTV) margins (Eijkelenkamp, Boekhoff et al., 2021; Yang, Yuan et al., 2022). Furthermore, these approaches did not incorporate real-time, patient-specific motion data and often fail to account for inter-patient variability in tumor motion and proximity to organs-at-risk (OARs).

Therefore, this study aims to perform a detailed analysis on the effects of gating envelop size on treatment efficiency and normal tissue sparing, providing a basis for developing a personalized margin determination strategy for automatic gating in MRIgRT. By performing motion and dosimetric analyses using cine MR images acquired during MRIgRT in patients with HCC, we propose clinically applicable guidelines for patient-specific GE definition. Multiple patient-specific characteristics, such as GTV size and spatial relationship between GTV and OARs, were considered in the dosimetric analysis.

2. Material and Methods

2.1. Patient Selection and Imaging Acquisition

This retrospective single-institutional study included ten patients with HCC who received MRIgRT between January and December 2024 (IRB No. 2024-1252-001). Inclusion criteria required availability of cine MRI before and after treatment and analyzable tumor motion profiles; patients with unstable breathing or significant imaging artifacts were excluded. The cohort had a mean age of 62.7 years (range: 52-74), consisting of 7 males and 3 females. Tumors were located in the right hepatic lobe (6 patients), left lobe (3), and hepatic hilum (1), with a mean GTV volume of 115.6 ± 144.3 cc (range: 6.4-435.2 cc) as summarized in Table 1.

All patients were immobilized using a WingSTEP® arm support (Elekta AB, Stockholm, Sweden), KneeSTEP® leg support (Elekta AB, Stockholm, Sweden), and ZiFix ™ chest compression system (QFix, Avondale, USA) during imaging and treatment. Three-dimensional CT (3D CT) scans (1-3 mm slice thickness) were acquired for treatment planning. Four-dimensional CT (4D CT) scans were acquired to assess respiratory motion and were reconstructed into ten respiratory phase. All CT scans were acquired using a CT simulator, SOMATOM Definition AS (Siemens Healthineers, Erlangen, Germany).

Real-time cine MRI was acquired using the Unity MR-Linac system (Elekta AB, Stockholm, Sweden), which integrates a 1.5 T magnetic resonance imaging scanner with a linear accelerator for MRIgRT. During-treatment imaging was performed in sagittal, coronal, and axial planes using a balanced turbo Field Echo sequence at approximately 5 frames per second, providing a sufficient time resolution to continuously capture respiratory motions. Since cine MR acquisition was not conducted in some treatment sessions, a total of 67 cine MR image sets were included in the motion tracking analysis.

Table 1. Summary of patient characteristics.

Patient	Age	Sex	Tumor location (liver segment)	Dose fractionation (Gy × fractions)	GTV volume (cc)
1	45	F	S4/S7/8	10.0 × 5	26.7
2	66	F	S4	3.0 × 10	11.5
3	78	M	S5/8	3.7 × 10	82.8
4	75	M	S4/8	4.0 × 10	62.7
5	65	M	S5/8	6.5 × 10	13.3
6	69	M	S4/3	4.0 × 10	224.6
7	59	M	S1/6	4.0 × 10	31.4
8	65	F	S1	13.0 × 3	6.4
9	63	F	Right posterior liver	4.0 × 10	435.2
10	55	M	S6	2.1 × 25	261.7

Note: Liver segment, where tumor was located, was identified based on radiologic assessment.
Abbreviations: gross tumor volume, GTV.

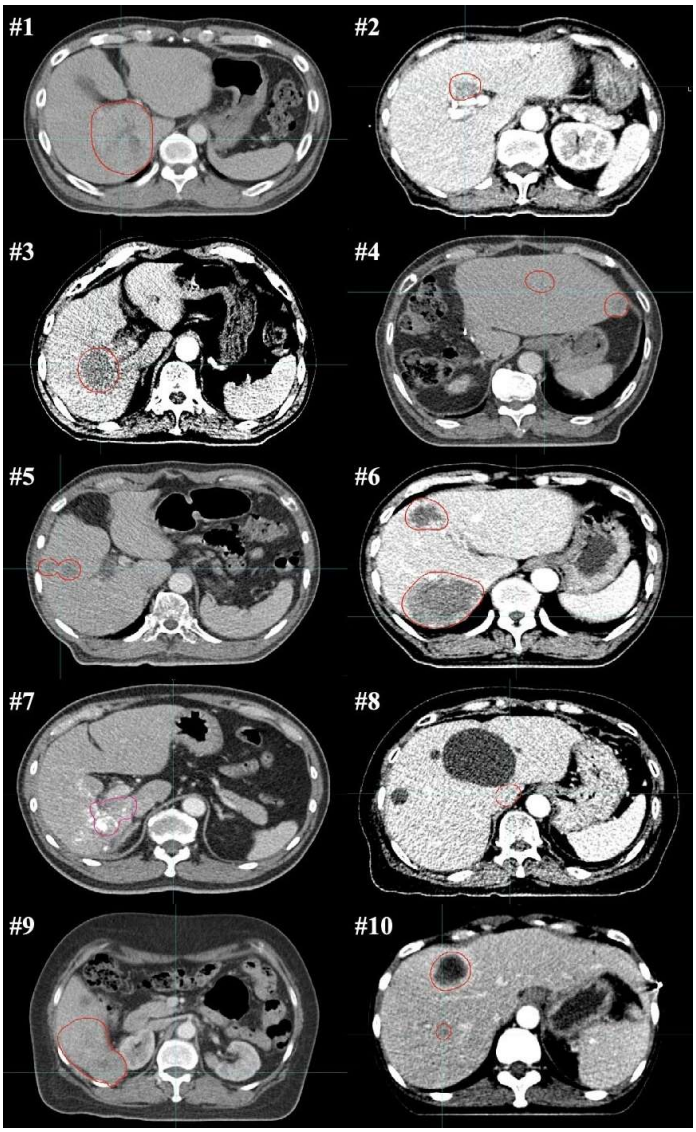

Figure 1. Axial 3D planning CT images showing the GTV (red contour) for each of the 10 patients.

2.2. Definition of Gating Envelopes

For each of the patients, GTV was manually delineated by a professional radiation oncologist based on CT and MRI images. The GTVs delineated for all patients are graphically represented in Figure 1. For the radiation treatment, ITV was generated by expanding the GTV to cover the entire range of respiratory motions observed in 4D CT (all-phase (0-90%)).

To investigate the potential need of personalized GE determination, in addition to the ITV by the ITV approach, we defined three gated ITVs, each covering a specific range of respiratory phases: 1) 7-phase (20-80%), 2) 5-Phase (30-70%), and 3) 3-Phase (40-60%) (Figure 2). For gating treatment (excluding all-phase case), GEs were created by adding a 2 mm isotropic margin to the gated ITVs, which corresponds to the rigid registration uncertainty in a vendor-provided motion tracking analysis tool reported by a previous study (Keiper, Tai et al. 2020). The vendor-provided motion tracking analysis tool used in this study is described in detail in Section 2.4. Consequently, three different GEs were defined: 1) 7-phase GE, 2) 5-phase GE, and 3) 3-phase GE.

For OARs, including the liver (excluding GTV), bowel, stomach, duodenum, kidneys, and spinal cord, planning risk volumes (PRVs) were contoured to account for respiratory motions.

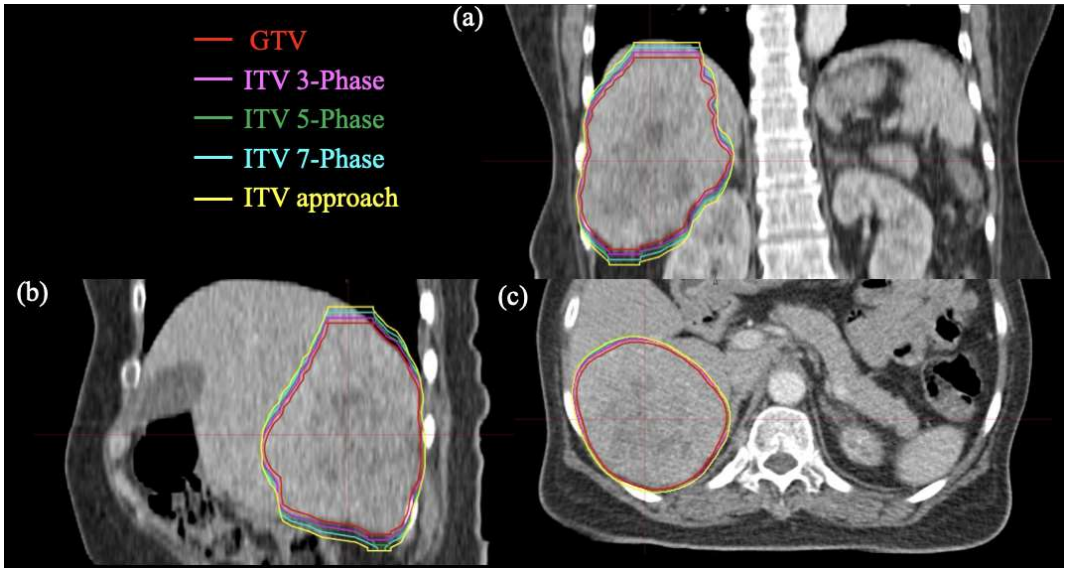

Figure 2. (a) Coronal, (b) sagittal, and (c) axial CT images illustrating the GTV (red) and ITVs generated to cover different ranges of respiratory phases: ITV (0-90%, yellow), ITV 7-phase (20-80%, cyan), ITV 5-phase (30-70%, green), and ITV 3-phase (40-60%, pink). Abbreviations: gross tumor volume, GTV; internal target volume, ITV.

2.3. Dosimetric Analysis

All treatment plans were generated using step and shoot IMRT on the Unity MR-Linac system (Elekta AB, Stockholm, Sweden). Dose calculations were performed using the Monaco treatment planning system (version 5.51, Elekta AB, Stockholm, Sweden), employing a Monte Carlo algorithm with a 2-3 mm grid resolution.

In addition to the radiation treatment plan delivered for the actual treatment, which was based on the all-phase ITV, additional treatment plans were generated for the three additional GEs. For the ITV-based approach, planning target volume was created by adding a margin of 2 mm to the ITV. Each plan was optimized to ensure adequate target coverage: $D_{95} \geq 100\%$ of the prescribed dose for the PTV in the ITV-based approach and for the GEs in the gating treatment, respectively. Dose constraints were applied in accordance with the Quantitative Analyses of Normal Tissue Effects in the Clinic (QUANTEC) guidelines (Bentzen et al., 2010), as summarized in Table 2. These dosimetric thresholds were tailored to various fractionation schemes.

Table 2. Dose constraints for the liver and gastrointestinal OARs for various dose fractionation schemes based on the QUANTEC guidelines.

Fractionation Scheme	OAR	Dose Constraint
3-Fraction SBRT	Non-tumor liver	≥700 cc must receive ≤15 Gy
	Stomach/Duodenum	D_{max} <30-35 Gy
	Small Bowel	D_{max} <30 Gy
6-Fraction SBRT	Non-tumor liver	≥700 cc must receive ≤18 Gy
	Stomach/Duodenum	D_{max} <30-35 Gy
	Small Bowel	D_{max} <30 Gy
Conventional	Liver	Mean liver dose ≤28 Gy
	Stomach/Duodenum	D_{max} <54 Gy
	Small Bowel	D_{max} <52 Gy

Abbreviations: organ-at-risk, OAR; stereotactic body radiation therapy, SBRT; maximum dose, Dmax; Quantitative Analyses of Normal Tissue Effects in the Clinic, QUANTEC.

All treatment plans were evaluated using dose-volume histogram (DVH) metrics, including D95 (minimum dose that 95% of volume-of-interest receives), mean dose (D_{mean}), and maximum dose (D_{max}) of the target volume (PTV for the ITV-based approach and GE for the gating treatment).

To analyze the impact of target volume (i.e., GE size) on the liver mean dose, a normalized liver mean dose (D_{norm}) was defined as the ratio of the liver mean dose in a gating plan to that in the ITV-based plan as shown in Equation (1):

$$D_{norm}(\%) = \frac{D_{mean}(liver, gating\,plan)}{D_{mean}(liver, Vplan)} \times 100 \quad (1)$$

Since the dose fractionation schemes varied across the patients, the level of reduction in the dose delivered to the liver can be effectively evaluated by normalizing the liver dose as described in Equation (1). Additionally, the relationship between the GTV volume and the liver dose was analyzed to determine the extent to which tumor size influences the effectiveness of different GE strategies. Compliance with the QUANTEC liver dose constraints was analyzed in relation to the GE definition and individual GTV volume.

While the doses to other OARs, such as stomach, duodenum, and bowel, were normalized to the prescription dose, the impact of an additional factor on the OAR doses was taken into consideration: the distance between the target and the OAR, referred to as the GTV-to-OAR distance. To calculate the GTV-to-OAR distance, the minimum Euclidean distance to each of nearby OARs was computed by performing a series of isotropic expansions of the GTV with various margin sizes as illustrated in Figure 3. This GTV-to-OAR distance computation was conducted for several OARs (stomach, duodenum, and bowel) using a commercial software (MIM Maestro, MIM Software Inc., Cleveland, OH, USA). It is noted that when the GTV and the OAR were overlapped, a negative value was assigned to the GTV-to-OAR distance.

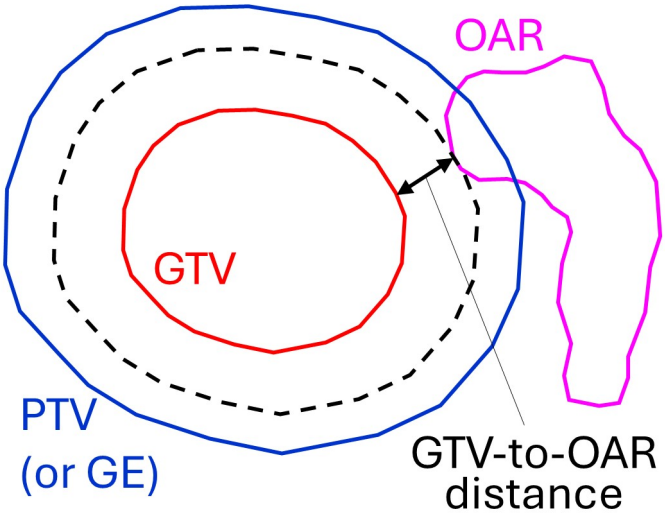

Figure 3. Schematic illustration of the GTV-to-OAR distance. The dashed line represents a uniformly expanded contour from the GTV, where the expansion continues until the expanded contour becomes tangent to the OAR contour. In this illustrative case, where the OAR overlapps with the PTV, a negative value is assigned to the GTV-to-OAR distance.
Abbreviations: gross tumor volume, GTV; organ-at-risk, OAR; planning target volume, PTV; gating envelope, GE.

2.4. Simulation of Automatic Gating Treatment

Automatic gating in MRIgRT was simulated using a vendor-provided motion tracking software package, Motion Monitoring Research Package (MMRP, Elekta AB, Stockholm, Sweden) as described in Figure 4. In this software package, tracking of a radiation target is achieved by performing a 3 degrees-of-freedom rigid image registration for a specific region-of-interest. It is noted that the region-of-interest for the image registration can be set as the target volume or a surrogate structure (e.g., liver for patients with HCC). In this study, the GTV was used as the region-of-interest for the rigid image registration since it was mostly visible on the cine MR images. As a result of the registration-based tracking, the shifts of the GTV in three directions are obtained and, therefore, time-dependent tumor motion can be visualized in the software package as in Figure 4.

Beam-on-time efficiency was calculated using MMRP, which was defined as the ratio of the beam-on-time to the total treatment time (i.e., the sum of beam-on and beam-off times). In other words, the beam-on-time efficiency, defined in this study, represents the percentage of the treatment time during which the GTV remains within the GE and radiation is actively delivered (also referred to as duty cycle in the literature). For each GE configuration, mean and standard deviation of the beam-on-time efficiency were calculated. One-way analysis of variance (ANOVA) was performed to evaluate statistical significance of differences in the beam-on-time efficiency between three GE groups, with Levene's test used to assess the equality of variances.

In addition, non-parametric correlation analyses were conducted by calculating Spearman's rank correlation coefficient to evaluate relationships between three parameters (the GE size, the GTV volume, and the tumor motion magnitude in the superior-inferior (SI) direction) and the beam-on-time efficiency. All statistical tests were two-sided with a significance level of $p < 0.05$, and analyses were performed using IBM SPSS Statistics (version 27.0.1; IBM Corp., Armonk, NY, USA).

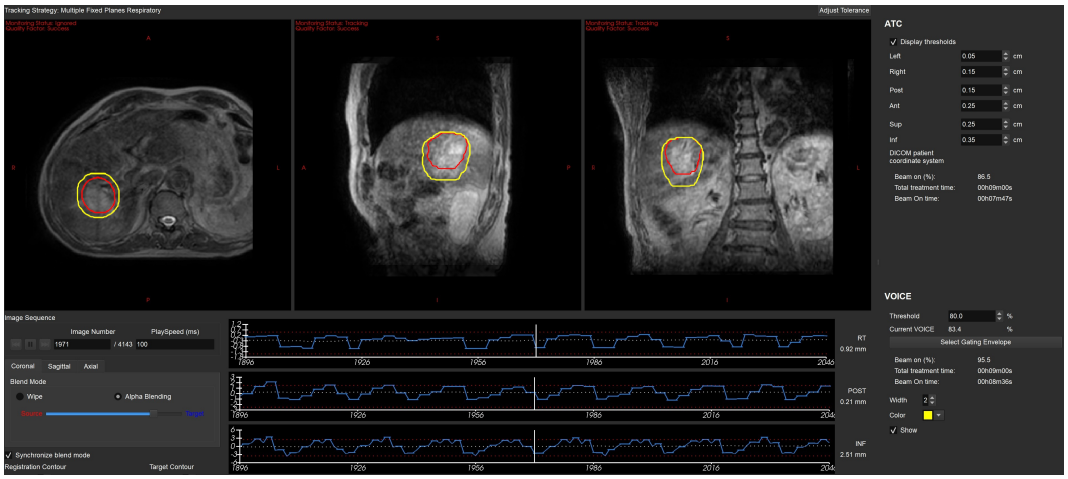

(a)

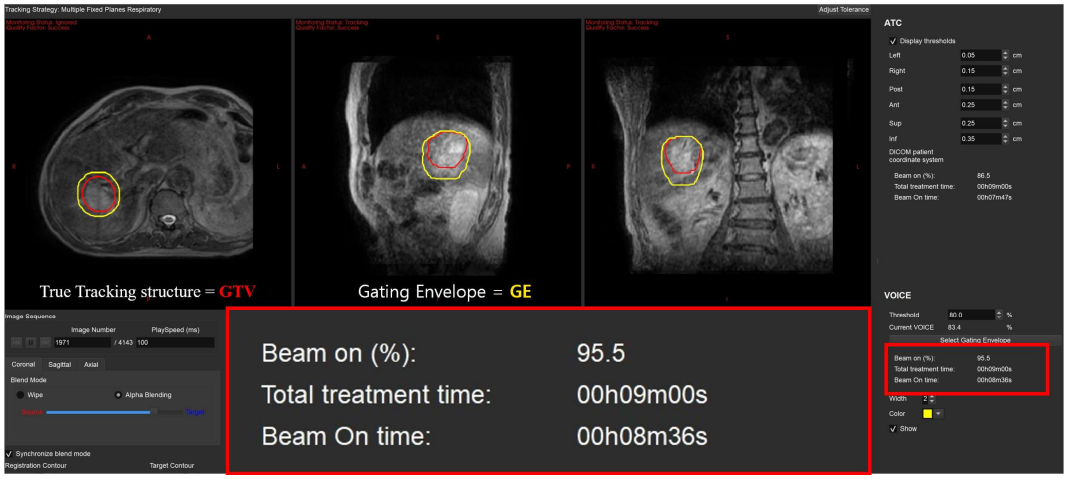

(b)

Figure 4. Operational view of a vendor-provided motion tracking software package, Motion Monitoring Research Package (MMRP), where the upper panel displays axial, sagittal, and coronal cine MR images with the GTV (red) and the GE (yellow) overlaid, and the lower panel shows (a) motion tracking results (translations) in three directions and (b) calculation results of beam-on-time efficiency (represented as beam on (%) in MMRP), total treatment time, and beam-on-time.
Abbreviations: gross tumor volume, GTV; gating envelope, GE.

2.5. Case-Specific Analysis

To examine the clinical utility of patient-specific GE optimization in greater detail, three representative cases (four patients: Patients 1, 3, 6, and 9) were selected based on distinct anatomical locations or motion characteristics. These cases involved:

Case I) Patient 1: patient case with a tumor adjacent to the liver dome,

Case II) Patients 3 and 6: patient case with extensive tumor motion, and

Case III) Patient 9: patient case with a tumor in close proximity to OARs.

3. Results

3.1. Dosimetric Impact of Gating Envelope Size

Comparisons of DVH metrics between the treatment plans with different target definitions are presented in Table 3. All treatment plans achieved adequate target coverage with D_{95} values $\geq$ 95% and showed similar plan quality in overall. Among the GE groups, the treatment plans based on the 5-phase and 3-phase GEs showed the highest D95 values (103.3% for both GEs), although the 3-phase GE group exhibited greater inter-patient variability. The maximum dose values were consistent across all GE groups (116.5-117.5%). The mean dose to the target ranged from 108.6% to 108.7%, exhibiting minimal variations across the treatment plans.

Table 3. Comparison of target dose parameters across different motion management techniques: ITV approach and respiratory gating with various GE configurations. Values are presented as mean ± standard deviation.

DVH metric	ITV approach	Gating treatment		
		7-phase	5-phase	3-phase
D_{95}(%)	100.9 ± 2.6	101.2 ± 4.6	103.3 ± 8.2	103.3 ± 8.3
D_{max}(%)	117.3 ± 12.3	116.6 ± 12.0	116.8 ± 12.2	116.8 ± 12.3
D_{mean}(%)	108.7 ± 9.5	108.6 ± 9.5	108.6 ± 9.7	108.6 ± 9.8

Note: D_{95} denotes inimum dose that 95% of volume-of-interest receives, normalized to the prescription dose, D_{max} denotes maximum dose, and D_{mean} denotes mean dose.
Abbreviations: internal target volume, ITV; gating envelope, GE; dose-volume histogram, DVH.

Figure 5 shows the normalized liver mean dose for each of the patients. The liver mean dose decreased as the phase range of the GE narrowed although the degree of the reduction varied across the patients. Compared to the ITV-based treatment plan (non-gated plan), the following average dose reductions were observed: 8.2% for 7-phase, 13.1% for 5-phase, and 15.4% for 3-phase GE, respectivly. Apparently, 3-phase GE, which corresponded to the smallest target definition, consistently achieved the greatest liver dose reduction across patients. Notably, Patients 1, 4, 7, and 8 experienced reductions exceeding 21%, indicating a strong individual benefit from phase-constrained gating.

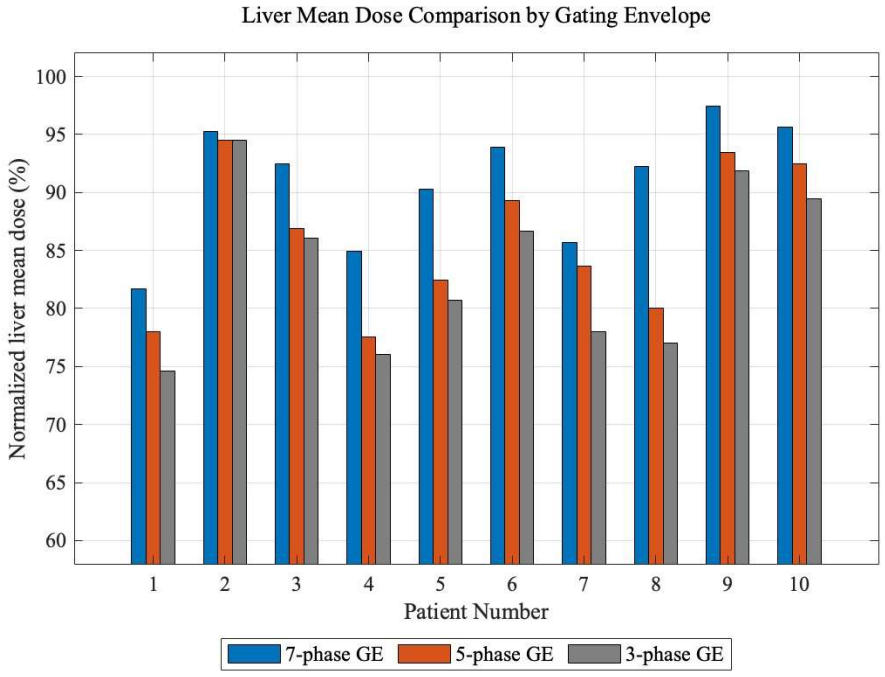

Figure 5. Comparison of the liver mean dose normalized to that of the ITV-based treatment plan between three GE conditions—7-phase GE (blue), 5-phase GE (orange), and 3-phase GE (gray).

In Figure 6, the liver mean dose values calculated for all patients are plotted against the GTV volume. As shown in Figure 6, patients with smaller GTVs (<100 cc) demonstrated better adherence to the QUANTEC liver dose constraints under tighter GE strategies. In contrast, patients with large GTVs (>150 cc) exceeded the dose limits regardless of the GE size, suggesting limited benefit from gating adjustments alone in such cases. Furthermore, a wider GE phase range was associated with higher absolute liver doses but reduced inter-patient variability.

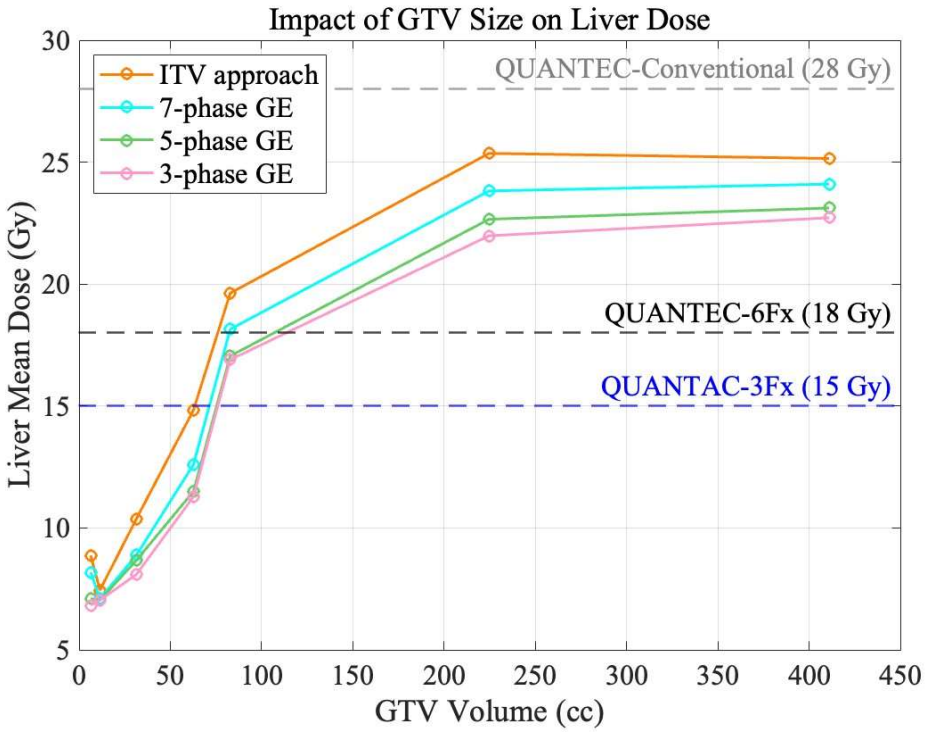

Figure 6. Liver mean dose as a function of GTV volume under different motion management strategies: ITV approach (orange), 7-phase GE (cyan), 5-phase GE (green), and 3-phase GE (pink). Horizontal dashed lines indicate QUANTEC liver dose limits: 28 Gy (gray), 18 Gy (black), and 15 Gy (blue), respectively.

In Table 4, the GTV-to-OAR distances calculated for the stomach, duodenum, and bowel are summarized for all patients. The GTV-to-OAR distances showed large variations across the patients. For instance, the distance to the stomach ranged from 0.0 to 5.3 cm. In the patient cohort, the GTV-to-OAR distance was smallest for the bowel; for 8 out 10 patients, the distance was less than 1 cm, with a maximum value of 3.1 cm. In four patient cases, an overlap between the GTV and at least one of the OARs was observed.

In Figure 7, the OAR doses normalized to the prescription doses for the stomach, duodenum, and bowel are plotted against the GTV-to-OAR distance. As illustrated in Figure 7, a shorter distance between the GTV and surrounding OARs was associated with increased OAR dose. Notably, when the GTV-to-OAR minimum distance was less than 1 cm, the OAR dose frequently exceeded 80% of the prescription dose, regardless of the GE size. However, treatment plans utilizing the 3-phase GE condition demonstrated substantial dose reduction by restricting beam delivery to a relatively narrow range of tumor positions.

Table 4. Minimum distances between the GTV and adjacent OARs (stomach, duodenum, and bowel). Negative values indicate volumetric overlap between the radiation target (.e., PTV for ITV approach or GE for gating treatment) and the OAR.

Patient#	GTV-to-OAR distance (cm)		
	Stomach	Duodenum	Bowel
1	5.3	7.0	-
2	0.0	2.6	0.4
3	1.0	1.7	0.5
4	0.6	8.6	0.7
5	3.8	-	1.7
6	3.4	3.1	3.1
7	1.6	-0.2	0.9
8	0.6	-	-
9	2.0	0.9	0.1
10	0.6	0.0	0.7

Abbreviations: gross tumor volume, GTV; organ-at-risk, OAR; planning target volume, PTV; gating envelope, GE.

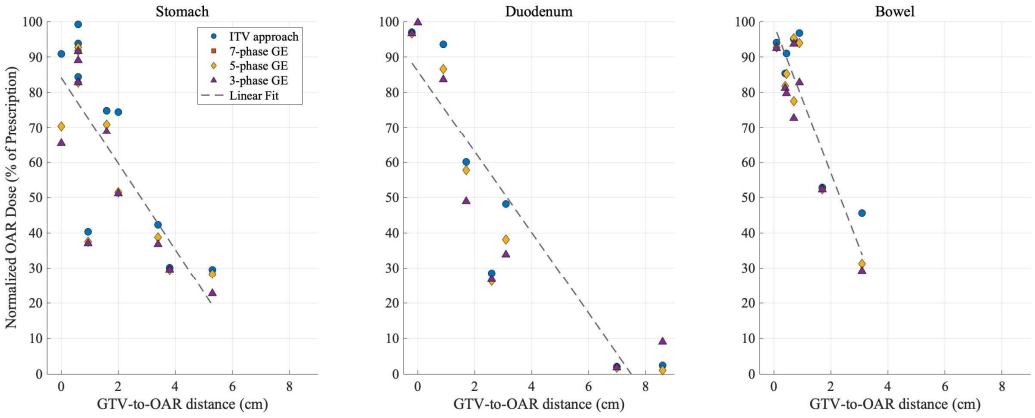

Figure 7. Normalized OAR doses (% of the prescription dose) plotted against the GTV-to-OAR distance (cm) for the stomach, duodenum, and bowel. Each data point represents one of four motion management techniques: ITV approach, gating treatment techniques with 7-phase, 5-phase, and 3-phase GEs.
Abbreviations: gross tumor volume, GTV; organ-at-risk, OAR; gating envelope, GE.

3.2. Impact on Beam-on-Time Efficiency

In Figure 8, the beam-on-time efficiency values calculated using MMRP for all patients are presented for each of the GE group. As shown in the box plots in Figure 8, the beam-on-time efficiency was highest for the plans using the 7-phase GE, followed by the 5-phase and the 3-phase GE configurations. The range of the beam-on-time efficiency values was broarder for smaller GE configuration.

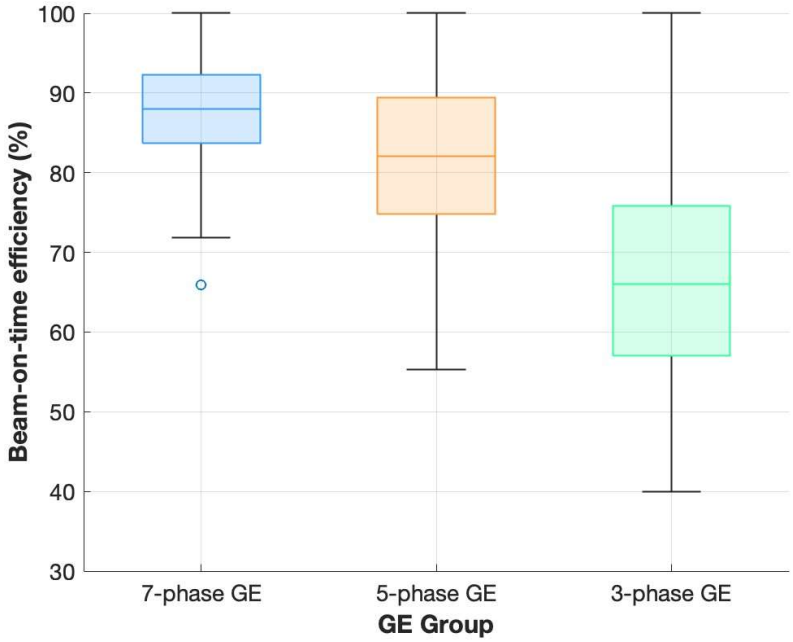

Figure 8. Box plot of comparing beam-on-time efficiency values calculated for all patients between three GE groups.
Abbreviations: gating envelop, GE.

Table 5. Statistics of beam-on-time efficiency values calculated across all patients for each of the GE configurations.

Gating envelope configuration	Beam-on-time efficiency (%)				
	Mean	SD	95% CI	Minimum	Maximum
7-phase GE	80.9	7.8	87.3-91.1	63.5	97.7
5-phase GE	82.3	10.9	79.7-85.0	56.7	96.2
3-phase GE	67.4	14.9	63.8-70.9	36.7	93.8

Abbreviations: standard deviation, SD; confidence interval, CI; gating envelope, GE; internal target volume, ITV.

Table 6. Summary of the correlation analysis between various factors (GE sizes, GTV volume, and tumor motion magnitude in the SI direction (SI motion magnitude)): Spearman's rank correlation coefficients and the corresponding p-values.

Factors	Correlation with beam-on-time efficiency	
	Spearman's rank correlation coefficient	p-value
GE configuration	−0.645	<0.001
GTV volume	0.093	0.180
SI motion magnitude	−0.104	0.135

Abbreviations: gating envelope, GE; gross tumor volume, GTV; superior-inferior, SI.

Statistics of the beam-on-time efficiency values are summarized for all GE configurations in Table 5. The Levene's test revealed significant differences in variance among the three GE groups ($p < 0.001$), indicating the violation of the equal-variance condition required for the classic ANOVA. Therefore, the Welch's ANOVA was performed, showing that the beam-on-time efficiency was significantly different between each pair of the three GE groups. Specifically, the following Games-Howell post-hoc analysis revealed significant differences in mean beam-on-time between: (1) $p < 0.001$ for the 7-phase vs. 5-phase GEs, (2) $p < 0.001$ for the 5-phase vs. 3-phase GEs, and (3) $p <$

0.001 for the 7-phase vs. 3-phase GEs, respectively.

Table 6 presents correlation analysis results between several factors, such as the GE size, the GTV volume, and the tumor motion magnitude in the SI direction, and the beam-on-time efficiency. There was a strong inverse relationship between the GE size and the beam-on-time efficiency as demonstrated in a Spearman's rank correlation coefficient of −0.645 ($p < 0.001$). Interestingly, no significant correlation was identified between the other factors (the GTV volume and the SI motion magnitude) and the beam-on-time efficiency as observed in the resulting correlation coefficients of 0.093 and −0.104, respectively.

3.3. Case-Specific Analysis

3.3.1. Case I: Tumor adjacent to the liver dome

As illustrated in Figure 9, for Patient 1, a tumor was located near the liver dome, a region typically subject to large diaphragmatic motion. The motion magnitude in the SI direction was relatively small for this patient (3 mm), possibly due to the use of the chest compression device. The beam-on-time efficiency for this patient was calculated as 81.7% with the 7-phase GE and 74.6% with the 3-phase GE. Although these values did not fall within the 95% confidence intervals observed across the entire patient cohort: 87.3-91.1% for the 7-phase GE and 63.8-70.9% for the 3-phase GE, respectively, a distinct trend in the beam-on-time efficiency was not found.

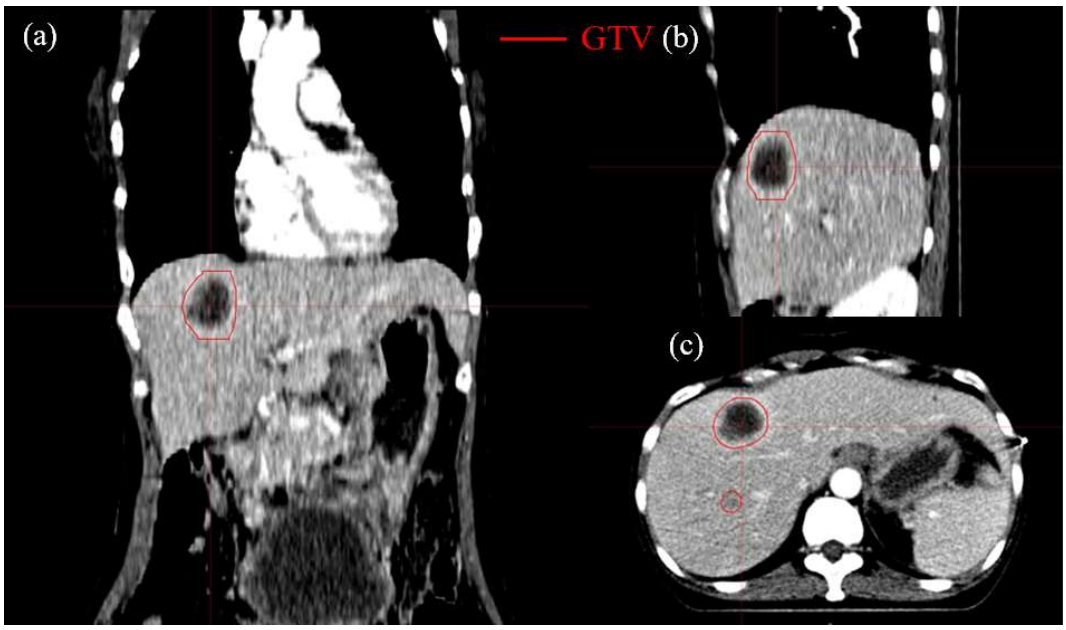

Figure 9. Representation of a patient case with a tumor adjacent to the liver dome (Patient 1), whose GTV contours are overlaid on (a) coronal, (b) sagittal, and (c) axial slices of the CT scan.
Abbreviations: gross tumor volume, GTV.

3.3.2. Case II: Extensive tumor motion

Figure 10 represents two representative cases (Patients 3 and 6) with relative large tumor motions. Patients 3 and 6 both exhibited large SI tumor motion, with amplitudes of approximately 15 and 10 mm, respectively. Although two patient cases showed large tumor motions, their beam-on-time efficiency under different GE settings differed markedly.

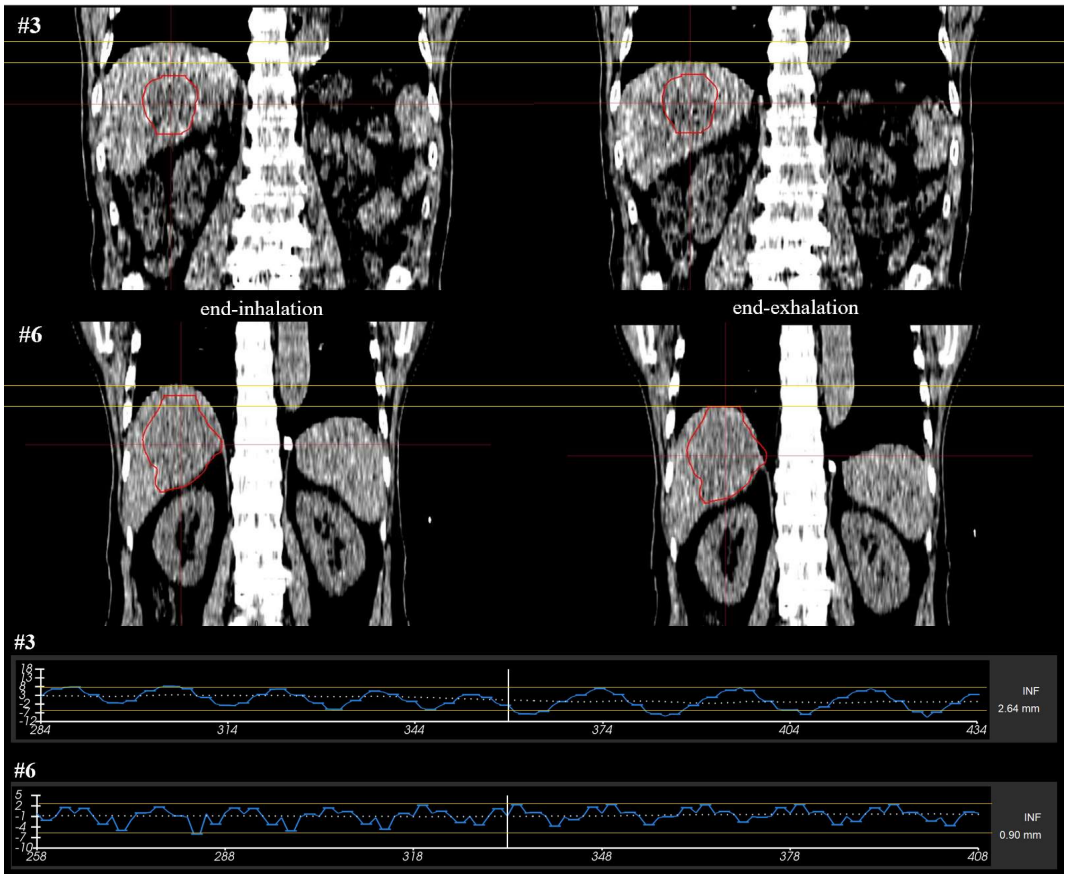

Figure 10. Representation of two representative cases (Patients 3 and 6) with relatively large tumor motions: coronal views of the 4D CT images at end-inhalation and end-exhalation respiratory phases (top panel), where two yellow lines represent the levels of the liver dome, and tumor motion traces in the superior-inferior direction (bottom).

Specifically, Patient 3 showed reduced efficiency, particularly under the 3-phase GE (49.9%), due to unexpected increases in respiratory amplitude during treatment that caused frequent tumor excursions outside the gating range. This mismatch between the predicted 4D CT motion and actual intra-fraction motion led to longer treatment times and lower efficiency. In contrast, Patient 6 maintained beam-on-time efficiency across all GE settings (85.8% for the 3-phase GE), demonstrating that the tumor motion remained well-contained within the GE predicted by 4D CT, with minimal deviation during delivery.

3.3.3. Case III: Tumor in close proximity to organs-at-risk

As illustrated in Figure 11, in Patient 9, the GTV was located in close proximity to major gastrointestinal OARs (stomach: 0.6 cm, duodenum: 0 cm, bowel: 0.7 cm). When the smallest GE (3-phase) was applied, substantial reductions in OAR dose were observed: 99.2% to 91.6% of the prescription dose for the stomach, 100.8% to 99.7% for the duodenum, and 100.1% to 93.7% for the bowel.

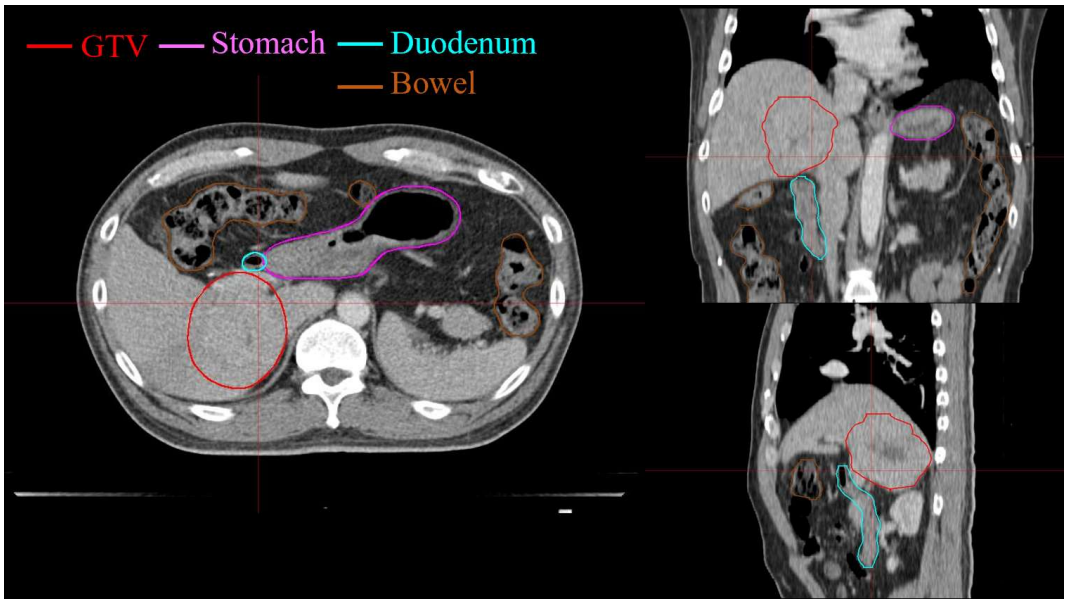

Figure 11. Representation of a patient case with a tumor in close proximity to gastrointestinal OARs (stomach, duodenum, and bowel); contours of the GTV and the OARs are overlaid on the axial (left), coronal (right-top), and sagittal (right-bottom) slices of the CT image.
Abbreviations: organ-at-risk, OAR; gross tumor volume, GTV.

4. Discussion

The findings in this study demonstrate that appropriate selection of GE size considering its dosimetric impact and beam delivery efficiency is particularly important for gating treatment in MRIgRT. To the best of the author's knowledge, this study is the first to investigate the impact of GE size on the resulting dose distribution and treatment time efficiency using real-time cine MR images acquired during MRIgRT. By moving beyond fixed-margin approaches, we demonstrate the potential need of personalized GE definition based on actual motion trajectories. Prior studies using the Elekta Unity MR-Linac system recommended static margins (e.g., 4 mm for rectal cancer) when treatment time was kept under 15 minutes (Eijkelenkamp, Boekhoff et al. 2021). Similarly, Yang and Yuan proposed anisotropic margins (LR: 2.8 mm, SI: 5.3 mm, AP: 3.9 mm) for prostate cancer (Yang, Yuan et al. 2022). However, these studies primarily focused on inter-fractional variations and did not incorporate intrafractional motion data from cine MRI into their margin size determination. Regarding the ViewRay MRIdian system, previous studies reported uniform breath-hold-based margins of 3-5 mm (Rogowski, von Bestenbostel et al. 2021; Ehrbar, Käser et al. 2022). Despite adaptive planning being applied in 98% of fractions in the study by Ehrbar et al., the margin remained fixed at GTV + 3 mm, without real-time motion-based adjustment. Furthermore, the reported average gating efficiency (~55%) reflects the limitations of static margin-based gating protocols.

Our results showed that while reducing the GE size led to decreased beam-on-time efficiency, it reduced radiation exposure to the liver and the OARs. This is a general statement that can be drawn from the findings presented in this study on the impact of the GE size on the resulting dose distributions and the treatment efficiency. Specifically, regarding the liver dose, the GE size is directly related to the normal liver volume. Therefore, it is anticipated that, in radiation treatment planning with a large GE size,

reducing the liver dose becomes more challenging. Similarly, since the study results demonstrate that the liver dose was greatly influenced by the GTV volume for patients with HCC, the GTV volume should be considered in the decision-making process for gating treatment in MRIgRT. Specifically, for patients with GTV volumes of 50-100 cc, the 3-phase (the smallest) GE strategy enabled liver dose reductions sufficient to meet the QUANTEC 3-fraction constraint (mean liver dose < 15 Gy) (Bentzen, Constine et al. 2010). On the other hand, for small GTV volumes, since a remaining normal liver volume is relatively large, it was not challenging to meet the QUANTEC dosimetric criteria, allowing larger degrees-of-freedom to make a decision on the GE size; possibly, an institution-specific clinical decision may be made considering both dosimetric effects and treatment efficiency.

Regarding the OAR doses, the study findings underscore the importance of incorporating anatomical relationships between the target and the OARs into treatment planning. When the GTV-to-OAR distance was <1 cm, the choice of GE had a greater impact on the resulting OAR doses. This was further demonstrated by a specific patient case (Patient 9), in which the stomach, duodenum, and bowel were located within 1 cm of the GTV. In this patient case, the maximum dose to the OARs was reduced by as much as 7.7% by using the 3-phase GE configuration, demonstrating the clinical value of individualized gating strategies in challenging anatomical situations.

Interestingly, while the treatment efficiency, evaluated by means of beam-on-time efficiency, was strongly influenced by the GE size, it was less affected by the GTV volume and tumor motion magnitude. This was illustrated by the two specific-case analyses (Case I and Case II). First, in Case I (Patient 1), in which a tumor was located adjacent to the liver dome, tumor motion was effectively mitigated using a chest compression device, despite the fact that large tumor motion is typically anticipated in this region. Although the tumor motion magnitude was relatively small in this patient, the resulting beam-on-time efficiency was comparable to those observed in the entire patient

cohort. The comparison of Patients 3 and 6, both of whom exhibited relatively large tumor motion (15 mm and 10 mm in the SI direction, respectively), illustrated that breathing pattern may play a more critical role than motion amplitude in influencing treatment efficiency. Patient 3 showed substantial discrepancy between predicted motion from 4DCT and actual motion seen in cine MRI, while Patient 6's motion was more consistent. The large difference in the beam-on-time efficiency between the two patients suggests that breathing pattern should be carefully considered when determining the appropriate GE configuration. The specific-case analysis result also suggests that 4D CT may not fully capture individual breathing dynamics, highlighting the limitations of using current standard planning data for real-time treatment decisions. Real-time cine MRI is therefore crucial for identifying such deviations and enabling accurate, patient-specific GE optimization in MR-guided radiotherapy.

Several limitations should be noted. First, this study included a relatively small patient cohort (10 patients). However, for the motion tracking analysis using MMRP, all available cine MR imaging data (imaging data from 67 treatment sessions in total) were utilized, helping to compensate for the limited sample size. Second, the motion tracking analysis was conducted using 2D cine MR images, not considering volumetric motions. Currently, cine MR images are limited to a series of 2D acquisitions. A future study may explore the development of 3D cine MR imaging to capture full 3D anatomical motion, as its potential has been demonstrated in previous research (Yoon, Chun et al. 2024).

5. Conclusions

This study presents a comprehensive evaluation of how GE configuration affects treatment efficiency and normal tissue sparing in MRIgRT for liver cancer, using real-time respiratory motion data from cine MRI. Through quantitative analysis, we found that optimal GE selection must be tailored to individual tumor characteristics—specifically, tumor volume and the spatial proximity between GTV and OARs. Findings in this study emphasize that fixed, uniform gating protocols are suboptimal, and that personalized, motion-informed GE design—derived from cine MRI tracking—can achieve a balance between treatment precision, efficiency, and safety. The proposed approach provides a clinically feasible framework for individualized MRIgRT, with potential applicability to other abdominal or thoracic tumors. Future studies incorporating 4D imaging, prospective clinical workflow integration, and long-term outcome evaluation will be necessary to fully validate and extend the utility of patient-specific GE strategies.

References

Bentzen, S. M., Constine, L. S., Deasy, J. O., Eisbruch, A., Jackson, A., Marks, L. B., Ten Haken, R. K., & Yorke, E. D. (2010). Quantitative analyses of normal tissue effects in the clinic (QUANTEC): An introduction to the scientific issues. *International Journal of Radiation Oncology, Biology, Physics, 76(3),* S3−S9. https://doi.org/10.1016/j.ijrobp.2009.09.040

Bucknell, N. W., Belderbos, J., Palma, D. A., lyengar, P., Samson, P., Chua, K., Gomez, D., McDonald, F., Faivre-Finn, C., Hanna, G. G., & Siva, S. (2022). Avoiding toxicity with lung radiation therapy:An IASLC perspective. *Journal of Thoracic Oncology*, *17(8),* 961-973. https://doi.org/10.1016/j.jtho.2022.05.003

Ehrbar, S., Braga Käser, S., Chamberlain, M., Krayenbühl, J., Wilke, L., Mayinger, M., Garcia Schüler, H., Guckenberger, M., Andratschke, N., & Tanadini-Lang, S. (2022). MR-guided beam gating: Residual motion, gating efficiency and dose reconstruction for stereotactic treatments of the liver and lung. *Radiotherapy and Oncology, 174,* 101−108. https://doi.org/10.1016/j.radonc.2022.07.007

Eijkelenkamp, H., Boekhoff, M. R., Verweij, M. E., Peters, F. P., Meijer, G. J., & Intven, M. P. W. (2021). Planning target volume margin assessment for online adaptive MR-guided dose-escalation in rectal cancer on a 1.5 T MR-Linac. *Radiotherapy and Oncology, 163,* 185−191. https://doi.org/10.1016/j.radonc.2021.07.011

Keiper, T. D., Tai, A., Chen, X., Paulson, E., Lathuilière, F., Bériault, S., Hébert, F., Cooper, D. T., Lachaine, M., & Li, X. A. (2020). Feasibility of real‐time motion tracking using cine MRI during MR‐guided radiation therapy for abdominal targets. *Medical Physics, 47(8),* 3554‐3566. https://doi.org/10.1002/mp.14230

Kishan, A, U., Ma, T. M., Lamb, J. M., Casado, M., Wilhalme, H., Low, D. A., Sheng, K., Sharma, S., Nickols, N. G., Pham, J., Yang, Y., Gao, Y., Neylon, J., Basehart, V., Cao, M., & Steinberg, M. L. (2023). Magnetic resonance imaging-guided vs computed tomography-guided stereotatic body radiotherapy for prostate cancer: The MIRAGE randomized clinical trial. *JAMA Oncology, 9(3),* 365-373. https://doi.org/10.1001/jamaoncol.2022.6558

Kong, M., & Hong, S. E. (2016). Comparison of survival rates between 3D conformal radiotherapy and intensity-modulated radiotherapy in patients with stage III non-small cell lung cancer. *OncoTargets and therapy, 9,* 7227-7234.

Rogowski, P., von Bestenbostel, R., Walter, F., Straub, K., Nierer, L., Kurz, C., Landry, G., Reine, M., Auernhammer, C. J., Belka, C., Niyazi, M., & Corradini, S. (2021). Feasibility and early clinical experience of online adaptive MR-guided radiotherpy of liver tumors. *Cancers, 13(7),* 1523. https://doi.org/10.3390/cancers13071523

Shirato, H., Shimizu, S., Kunieda, T., Kitamura, K., van He, M., Kagei, K., Nishioka, T., Hasimoto, S., Fujita, K., Aoyama, H., Tsuchiya, K., Kudo, K., & Miyasaka, K. (2000). Physical aspects of a real-time tumor-tracking system for gated radiotherapy. *International journal of Radiation Oncology, Biology, Physics, 48(4),* 1187-1195. https://doi.org/10.1016/S0360-3016(00)00748-3

Yang, B., Yuan, J., Poon, D. M. C., Geng, H., Lam, W. W., Cheung, K. Y., & Yu, S. K. (2022). Assessment of planning target volume margins in 1.5 T magnetic resonance-guided stereotactic body radiation therapy for localized prostate cancer. *Precision Radiation Oncology, 6(2),* 127−135. https://doi.org/10.1002/pro6.1155

Yoon, Y. H., Chun, J., Kiser, K., Marasini, S., Curcuru, A., Gach, H. M., Kim, J. S., Kim, T. (2024). Inter-scanner super-resolution of 3D cine MRI using a transfer-learning network for MRgRT. *Physics in Medicine and Biology*, *69(11)*, 115038. https://doi.org/10.1088/1361-6560/ad43ab

Abstract in Korean

자기공명영상 유도 자유호흡조절 방사선 치료에서 게이팅 영역 크기에 따른 선량 분포 및 치료 효율 영향

본 논문은 자유호흡(Free-breathing) 상태에서 실시간 cine MRI로 측정한 종양 움직임 데이터를 활용하여, 간암 환자의 자기공명영상 유도 방사선 치료(MRI-guided Radiation Therapy, MRIgRT)에서 환자 맞춤형 게이팅 영역(Gating Envelope, GE)의 설정이 정상조직 선량 분포, 치료 효율에 미치는 영향을 분석하는 것을 목적으로 한다. 기존의 고정된 경계(Margin) 및 게이팅 조건은 환자의 호흡 패턴이나 종양 위치 변화에 따라 정상조직의 과도한 피폭 또는 치료 시간의 비효율을 초래할 수 있다.

총 10명의 간암 환자를 대상으로, 후향적으로 4차원 전산화단층촬영(4D CT)과 실시간 자기공명영상(cine MRI)을 분석하였다. 종양의 움직임은 Motion Monitoring Research Package(MMRP)를 통해 정량화하였으며, 서로 다른 크기의 게이팅 영역(총 3종; 7-phase GE, 5-phase GE, 3-phase GE)을 적용하여 치료 상황을 가상 시뮬레이션하였다. 각 게이팅 영역 조건에 대해 beam-on-time efficiency, 간 평균 선량, 손상위험장기(Organ-at-Risk, OAR) 선량을 평가하였다.

분석 결과, 게이팅 영역 크기에 따라 치료 효율성과 정상조직 보호 간의 상충관계(trade-off)가 명확히 드러났다. 특히 종양 부피가 50-100 cc이며 손상위험장기와의 거리가 1 cm 미만인 경우, 3-phase GE 적용 시 간 평균 선량이 유의하게 감소하였다. 반대로 종양이 작고 손상위험장기와의 거리가 충분한 환자에서는 7-phase GE 설정을 통해 치료 시간을 단축하면서도 안전한 선량 분포 유지가 가능하였다.

본 연구는 자유호흡 상태에서 실시간 자기공명영상 기반 종양 움직임을 반영하여, 환자 맞춤형 게이팅 영역 설정이 가능한 정밀 방사선 치료 전략의 가능성을 제시한다. 향후 자동화된 게이팅 영역 설정 알고리즘 및 보정방사선치료계획(adaptive planning)과

연계한 연구를 통해 자기공명영상 유도 방사선 치료의 임상적 정밀도를 더욱 향상시킬 수 있을 것이다,

핵심되는 말: 자기공명영상 유도 방사선 치료(MRIgRT, MRI-guided Radiation Therapy), 실시간 자기공명영상(cine MRI), 간암, 게이팅 영역(Gating Envelope, GE), 자동 게이팅(Automatic Gating), 치료 효율(Treatment Efficiency), 정상조직 보호(Normal Tissue Sparing)